Report

Cell Reports

FMRP Modulates Neural Differentiation through m^{6}A-Dependent mRNA Nuclear Export

Graphical Abstract

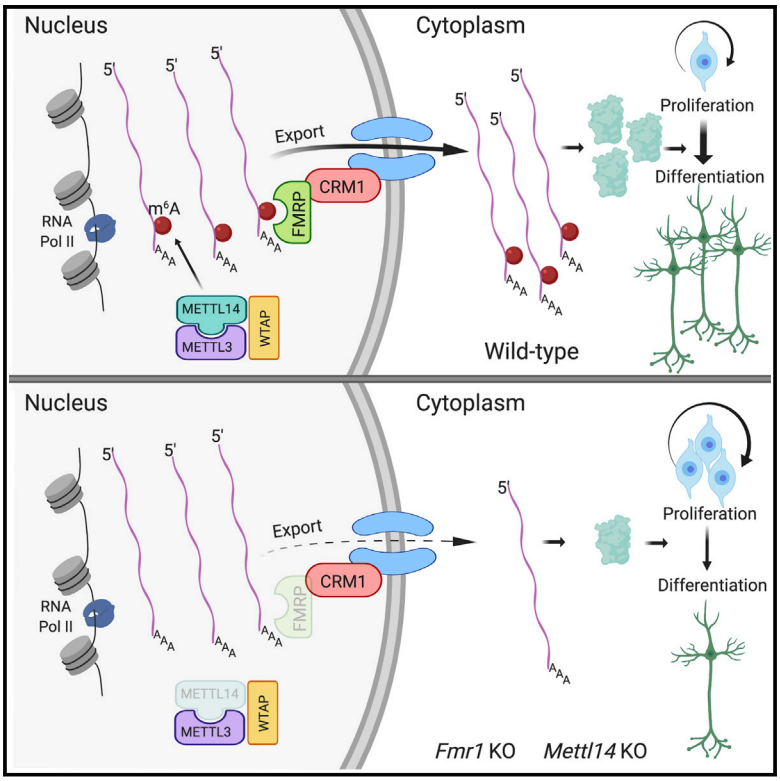

Highlights

- FMRP reads m^{6}A to promote mRNA nuclear export in neural differentiation
- Neural progenitor differentiation is delayed by knockout (KO) of *Fmr1* or *Mettl14*
- Both *Mettl14*KO and *Fmr1*KO lead to nuclear retention of m^{6}A-tagged FMRP target mRNAs
- FMRP preferentially binds m^{6}A-tagged mRNAs to facilitate nuclear export through CRM1

Authors

Brittany M. Edens, Caroline Vissers, Jing Su, ..., Chuan He, Hongjun Song, Yongchao C. Ma

Correspondence

shongjun@pennmedicine.upenn.edu (H.S.), ma@northwestern.edu (Y.C.M.)

In Brief

Edens et al. reveal fragile X mental retardation protein (FMRP) as an m^{6}A reader that promotes the nuclear export of methylated mRNAs during neural differentiation. Loss of either *Fmr1* or the m^{6}A methyltransferase *Mettl14* results in the nuclear accumulation of neural differentiation-related mRNAs, causing delayed neural progenitor differentiation in mice.

Edens et al., 2019, Cell Reports *28*, 845–854
July 23, 2019
https://doi.org/10.1016/j.celrep.2019.06.072

CellPress

Cell Reports
Report

FMRP Modulates Neural Differentiation through m^{6}A-Dependent mRNA Nuclear Export

Brittany M. Edens,[1,2] Caroline Vissers,[3] Jing Su,[1,2] Saravanan Arumugam,[1,2] Zhaofa Xu,[1,2] Han Shi,[1,2] Nimrod Miller,[1,2] Francisca Rojas Ringeling,[4] Guo-li Ming,[5] Chuan He,[6] Hongjun Song,[5,*] and Yongchao C. Ma[1,2,7,*]

[1]Departments of Pediatrics, Neurology, and Physiology, Northwestern University Feinberg School of Medicine, Chicago, IL 60611, USA
[2]Ann & Robert H. Lurie Children's Hospital of Chicago, Chicago, IL 60611, USA
[3]Biochemistry, Molecular and Cellular Biology Training Program, Johns Hopkins University School of Medicine, Baltimore, MD 21205, USA
[4]Gene Center, Ludwig-Maximilians-Universität München, Munich 81377, Germany
[5]Department of Neuroscience and Mahoney Institute for Neuroscience, Department of Cell and Developmental Biology, Institute for Regeneration, University of Pennsylvania, Philadelphia, PA 19104, USA
[6]Departments of Chemistry and Biochemistry and Molecular Biology, The University of Chicago, Chicago, IL 60637, USA
[7]Lead Contact
*Correspondence: shongjun@pennmedicine.upenn.edu (H.S.), ma@northwestern.edu (Y.C.M.)
https://doi.org/10.1016/j.celrep.2019.06.072

SUMMARY

N^6-methyladenosine (m^{6}A) modification of mRNA is emerging as a vital mechanism regulating RNA function. Here, we show that fragile X mental retardation protein (FMRP) reads m^{6}A to promote nuclear export of methylated mRNA targets during neural differentiation. *Fmr1* knockout (KO) mice show delayed neural progenitor cell cycle progression and extended maintenance of proliferating neural progenitors into postnatal stages, phenocopying methyltransferase *Mettl14* conditional KO (cKO) mice that have no m^{6}A modification. RNA-seq and m^{6}A-seq reveal that both *Mettl14*cKO and *Fmr1*KO lead to the nuclear retention of m^{6}A-modified FMRP target mRNAs regulating neural differentiation, indicating that both m^{6}A and FMRP are required for the nuclear export of methylated target mRNAs. FMRP preferentially binds m^{6}A-modified RNAs to facilitate their nuclear export through CRM1. The nuclear retention defect can be mitigated by wild-type but not nuclear export-deficient FMRP, establishing a critical role for FMRP in mediating m^{6}A-dependent mRNA nuclear export during neural differentiation.

INTRODUCTION

Methylation of RNA on N^6-adenosine (m^{6}A) is emerging as a critical mechanism regulating different aspects of RNA metabolism and function, including stability (Du et al., 2016; Ke et al., 2017; Wang et al., 2014), localization (Roundtree et al., 2017), and translation (Lin et al., 2016; Meyer et al., 2015; Wang et al., 2015). In mammals, methyltransferases METTL3 (methyltransferase-like 3) and METTL14 form a complex that mediates the addition of methyl groups to adenosines in target RNAs (Liu et al., 2014). Readers such as the YTH (YT521-B homology) domain containing proteins bind and interpret m^{6}A in a sequence-dependent manner (Dominissini et al., 2012; Wang et al., 2014; Xu et al., 2014). The presence of m^{6}A erasers has also been revealed, suggesting the complex and dynamic regulation of m^{6}A (Jia et al., 2011; Wei et al., 2018). The emerging biological functions regulated by m^{6}A include the proliferation and differentiation of embryonic (Batista et al., 2014; Geula et al., 2015) and neural stem cells (Wang et al., 2018; Yoon et al., 2017), as well as complex behaviors and processes such as circadian rhythms (Fustin et al., 2013), stress response (Engel et al., 2018), and learning (Koranda et al., 2018).

The RNA-binding protein fragile X mental retardation protein (FMRP) is encoded by the fragile X mental retardation gene (*FMR1*), mutations in which result in fragile X syndrome, the leading genetic cause of intellectual disability. FMRP contains both a nuclear localization sequence (NLS) and a nuclear export sequence (NES), and it is localized in both the nucleus and the cytoplasm (Eberhart et al., 1996; Kim et al., 2009). The best-studied function of FMRP is the negative regulation of mRNA translation; thus, fragile X syndrome may result in part from the aberrant expression of FMRP target genes (Darnell et al., 2011; Richter et al., 2015). Functionally, loss of *Fmr1* has been associated with abnormalities in cortical development and dendritic spine formation, which may contribute to aberrant learning and behavior in fragile X syndrome (Castrén et al., 2005; La Fata et al., 2014; Saffary and Xie, 2011; Shen et al., 2019; Tervonen et al., 2009).

Here, we report that FMRP binds m^{6}A-modified mRNAs and promotes their nuclear export to regulate neural differentiation. *Fmr1* knockout *(Fmr1*KO) mice show delayed cell cycle progression and neural differentiation, phenocopying methyltransferase *Mettl14* conditional KO *(Mettl14*cKO) mice that are devoid of m^{6}A modification (Yoon et al., 2017). Both *Mettl14*cKO and *Fmr1*KO lead to the nuclear retention of m^{6}A-modified FMRP target mRNAs regulating neural differentiation, including components of Notch and Hedgehog signaling pathways. FMRP preferentially binds m^{6}A-modified target mRNAs and cooperates with the nuclear export protein CRM1 to facilitate nuclear export. Nuclear retention of methylated FMRP target mRNAs in *Fmr1*KO can be mitigated by wild-type *Fmr1* but not NES-lacking

*Fmr1*ΔNES, suggesting that FMRP is sufficient to drive the nuclear export of m^{6}A-tagged FMRP target mRNAs, and this mechanism requires the NES-nuclear export. Our findings establish a role for FMRP in regulating m^{6}A-dependent mRNA nuclear export during neural differentiation.

RESULTS

Genetic KO of *Fmr1* Leads to Delayed Neural Progenitor Cell Cycle Progression

Target binding site analysis suggests that FMRP may bind to consensus RNA methylation motifs (Ascano et al., 2012; Fu et al., 2014). To test whether the genetic removal of *Fmr1* affects m^{6}A-related functions during development *in vivo*, we assessed cortical neural progenitor cell cycle progression, which is regulated by m^{6}A (Yoon et al., 2017). We exposed embryonic day 17.5 (E17.5) wild-type (WT) and *Fmr1*KO mouse embryos to 5-ethynyl-2′-deoxyuridine (EdU) for 24 h and then measured the cell cycle exit by assessing the colocalization of EdU with Ki-67, a marker of proliferation (Figure 1A). The number of cells that had exited the cell cycle within the 24 h of EdU exposure (Ki-67$^-$EdU$^+$) was significantly decreased in *Fmr1*KO mice compared to WT mice (Figure 1B), suggesting delayed neural progenitor cell cycle exit in *Fmr1*KO mice.

To explore progenitor cell cycle dynamics further, we exposed E17.5 mouse embryos to EdU for 2 h, followed by labeling with the radial glial cell (RGC) marker Pax6 and the mitotic marker phospho-histone H3 (pH3) (Figure 1C). Triple-labeled cells (pH3$^+$Pax6$^+$EdU$^+$) are RGCs that have progressed from S phase to M phase within the 2-h span of EdU exposure. Comparison of this population to the total Pax6$^+$EdU$^+$ population allows for the assessment of relative rates of cell cycle progression in RGCs. There was a significant reduction in the number of EdU$^+$ RGCs that had entered M phase (EdU$^+$PH3$^+$Pax6$^+$) in the *Fmr1*KO mouse cortex (Figure 1D), suggesting that cell cycle progression to M phase is delayed by the loss of *Fmr1 in vivo.*

Further analysis of cell cycle dynamics using flow cytometry revealed prolonged G2/M in cultured *Fmr1*KO neural precursor cells (NPCs) (Figures 1E and 1F). Following a 30-min EdU pulse and a 5-h incubation, there were significantly fewer divided *Fmr1*KO NPCs (2n DNA content), accompanied by a greater number of undivided NPCs (4n DNA content), compared to WT (Figure 1G). No difference was observed in EdU incorporation (Figure S1). These data indicate a delay in mitotic exit in *Fmr1*KO NPCs. Observations from these three experiments in *Fmr1*KO mice phenocopy altered cell cycle dynamics reported in methyltransferase *Mettl14*cKO mice that have no m^{6}A (Yoon et al., 2017), suggesting that FMRP mediates m^{6}A function during neural progenitor differentiation.

Genetic Deletion of *Fmr1* in Mice Results in Prolonged Maintenance of Proliferating Neural Progenitors in the Postnatal Mouse Cortex

Delayed cell cycle exit may lead to the extended maintenance of neural progenitors. During mouse cortical development, multipotent Pax6$^+$ RGCs and fate-restricted Tbr2$^+$ intermediate progenitors (INPs) are largely depleted by postnatal stages (Dwyer et al., 2016; Yoon et al., 2017). To test whether neural progenitors are maintained postnatally in *Fmr1*KO mice, we pulsed animals with EdU at postnatal day 5 (P5) and analyzed 2 days later at P7. A significant number of EdU$^+$Pax6$^+$ proliferating RGCs and EdU$^+$Tbr2$^+$ INPs were present in *Fmr1*KO mice, but very few were present in WT littermates (Figures 2A and 2B). In addition, we examined the maintenance of glial fibrillary acidic protein (GFAP)-expressing radial fibers, which are required for interkinetic nuclear migration and neural progenitor division (Solecki et al., 2004). These radial fibers are normally not maintained postnatally after the completion of cortical neurogenesis. Whereas there were few radial fibers spanning the cortical wall in WT mouse cortex, by P7 many were present in the *Fmr1*KO cortex (Figure S2A). These data indicate that *Fmr1*KO mice maintain proliferating neural progenitors into postnatal stages.

To further characterize the impact of *Fmr1* deletion on cortical development, we examined the number of Pax6$^+$ RGCs and Tbr2$^+$ INPs in WT and *Fmr1KO* mouse cortices at E17.5, P0, and P6. While differences in the numbers of RGCs and INPs were undetectable at E17.5, both populations showed significant increases in the *Fmr1KO* mouse cortex at P0 and P6 (Figures 2C–2E). No differences in the gross morphology of the cortex at embryonic or postnatal stages were detected (Figure S2B). These findings are very similar to the extended maintenance of the proliferating neural progenitors reported in *Mettl14*cKO mice, which are devoid of m^{6}A (Yoon et al., 2017). The neural differentiation abnormalities we identified in *Frm1*KO mice phenocopy the m^{6}A-dependent defects found in *Mettl14*cKO mice, suggesting a functional relation between FMRP and m^{6}A *in vivo*.

FMRP Preferentially Binds m^{6}A-Modified RNAs to Promote Their Nuclear Export during Neural Differentiation

As previous analyses have suggested that FMRP may bind to consensus RNA methylation motifs (Ascano et al., 2012; Edupuganti et al., 2017; Fu et al., 2014), we considered that FMRP could serve as an m^{6}A reader to bind and interpret m^{6}A to regulate RNA function. To test this possibility, we performed electrophoretic mobility shift assay (EMSA) and bio-layer interferometry analysis to assess the binding affinity of purified FMRP to RNA oligos containing an endogenous m^{6}A-modified sequence from mouse *Dll1* mRNA or a consensus m^{6}A motif. In both analyses, FMRP binding to RNA probes was significantly enhanced by m^{6}A methylation, suggesting that FMRP preferentially binds to methylated RNAs compared to non-methylated RNAs (Figures 3A, 3B, S3A, and S3B).

As an RNA-binding protein, FMRP localizes to both the nucleus and the cytoplasm (Eberhart et al., 1996; Kim et al., 2009). Therefore, we hypothesized that FMRP could mediate nuclear RNA export. To test this, we performed RNA sequencing (RNA-seq) to compare mRNA levels in WT and *Fmr1*KO NPC nuclear fractions (Figures S4A and S4B). We found that genes involved in cell differentiation, neural development (Figure 3C), and embryonic development (Figure S3C) were enriched in *Fmr1*KO nuclear fractions, suggesting nuclear retention of these mRNAs upon the loss of *Fmr1*.

To understand how the binding of FMRP to m^{6}A affects neural differentiation, we identified all of the mRNAs that are both m^{6}A tagged and differentially expressed in *Fmr1*KO NPC nucleus by comparing the above RNA-seq with m^{6}A-seq of mouse

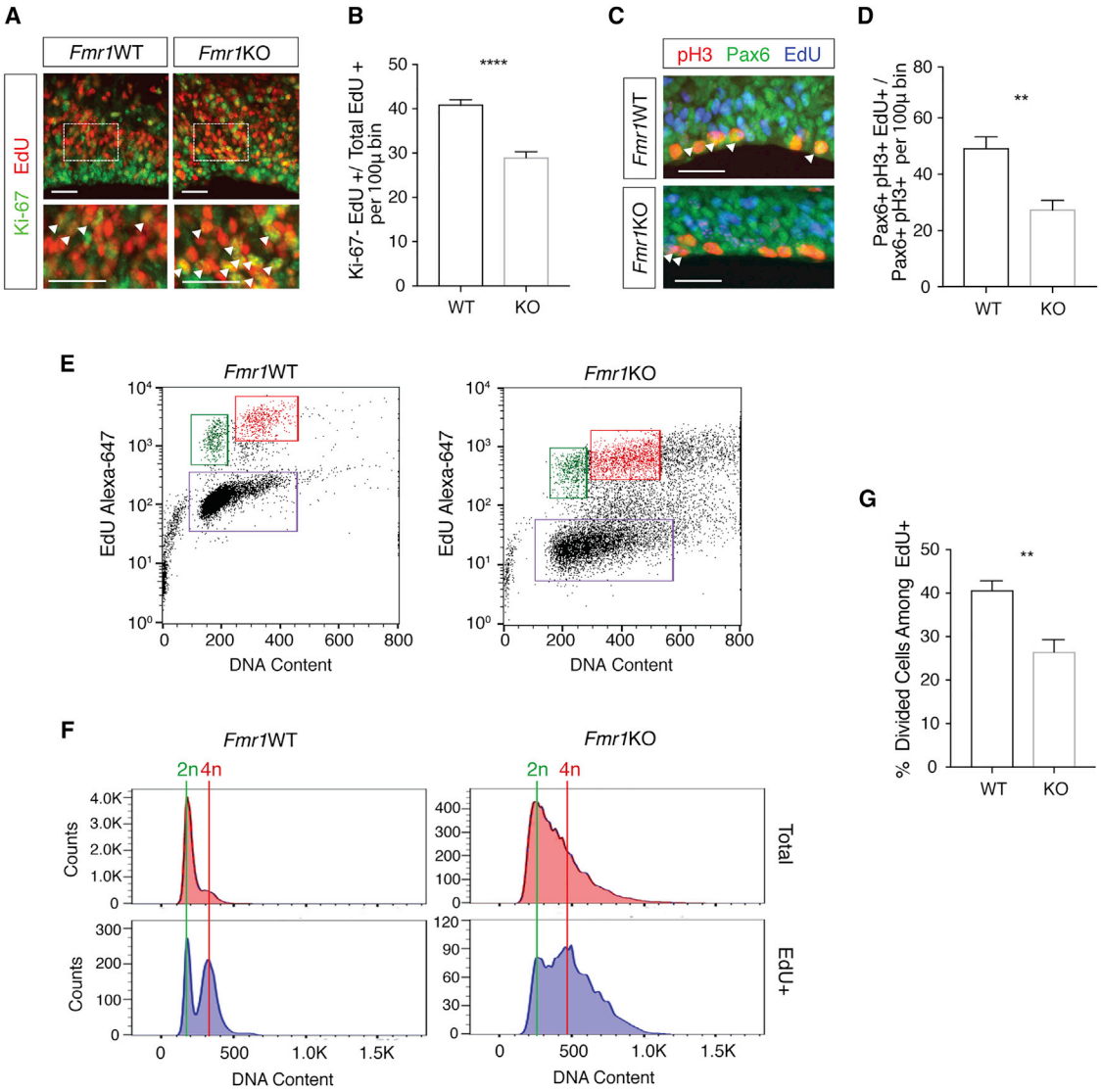

Figure 1. Genetic Knockout of *Fmr1* Leads to Delayed Neural Progenitor Cell Cycle Progression

(A) Analysis of cell cycle exit in WT and *Fmr1*KO E17.5 cortical progenitors. EdU (24 h) staining is shown in red and Ki-67 in green. Enlarged sections (bottom) highlight Ki-67^{+}EdU^{+} cells (arrows). Scale bars, 25 μm.

(B) Significantly fewer EdU^{+} cells exit the cell cycle during the 24-h EdU exposure in *Fmr1*KO cortex (****p $\leq$ 0.0001; n = 5 WT, 6 KO mice). Data are presented as mean + SEM.

(C) Analysis of M phase entry in WT and *Fmr1*KO cortical progenitors. pH3 staining is shown in red, Pax6 in green, and EdU in blue. Scale bar, 25 μm.

(D) Significantly fewer EdU^{+} RGCs entered mitosis within the 2-h EdU exposure in *Fmr1*KO cortex (**p = 0.0017; n = 6 WT, 6 KO mice). Data are presented as mean + SEM.

(E) FACS analysis of cell cycle dynamics in WT and *Fmr1*KO NPCs. Cells labeled by EdU are shown in the upper quadrants. Cells that divided during the 5-h incubation are shown in green and cells remaining in G2/M are in red.

(F) Histograms comparing 2n (divided) and 4n (undivided) NPCs between WT and *Fmr1*KO.

(G) Significantly fewer *Fmr1KO* EdU^{+} NPCs completed division by the end of 5 h compared to EdU^{+} WT NPCs (**p = 0.0018; n = 6 WT, 6 KO mice). Data are presented as mean + SEM.

embryonic neural progenitors (Figure 3D). Gene Ontology analysis revealed enrichment in processes such as neurogenesis, neural differentiation, and regulation of gene expression (Figure 3E), as well as chromatin and DNA binding (Figure S3D). Furthermore, pathway analysis yielded terms related to pluripotency and developmental signaling pathways (Figure 3F). Among the mRNAs that are both m^{6}A tagged and differentially expressed in *Fmr1*KO NPC nucleus, components of the Notch and Hedgehog pathways (Figures 3G and 3H) are particularly interesting, as they are involved in regulating the balance between neural stem cell maintenance and differentiation and have been genetically associated with intellectual disability (Chaudhry et al.,

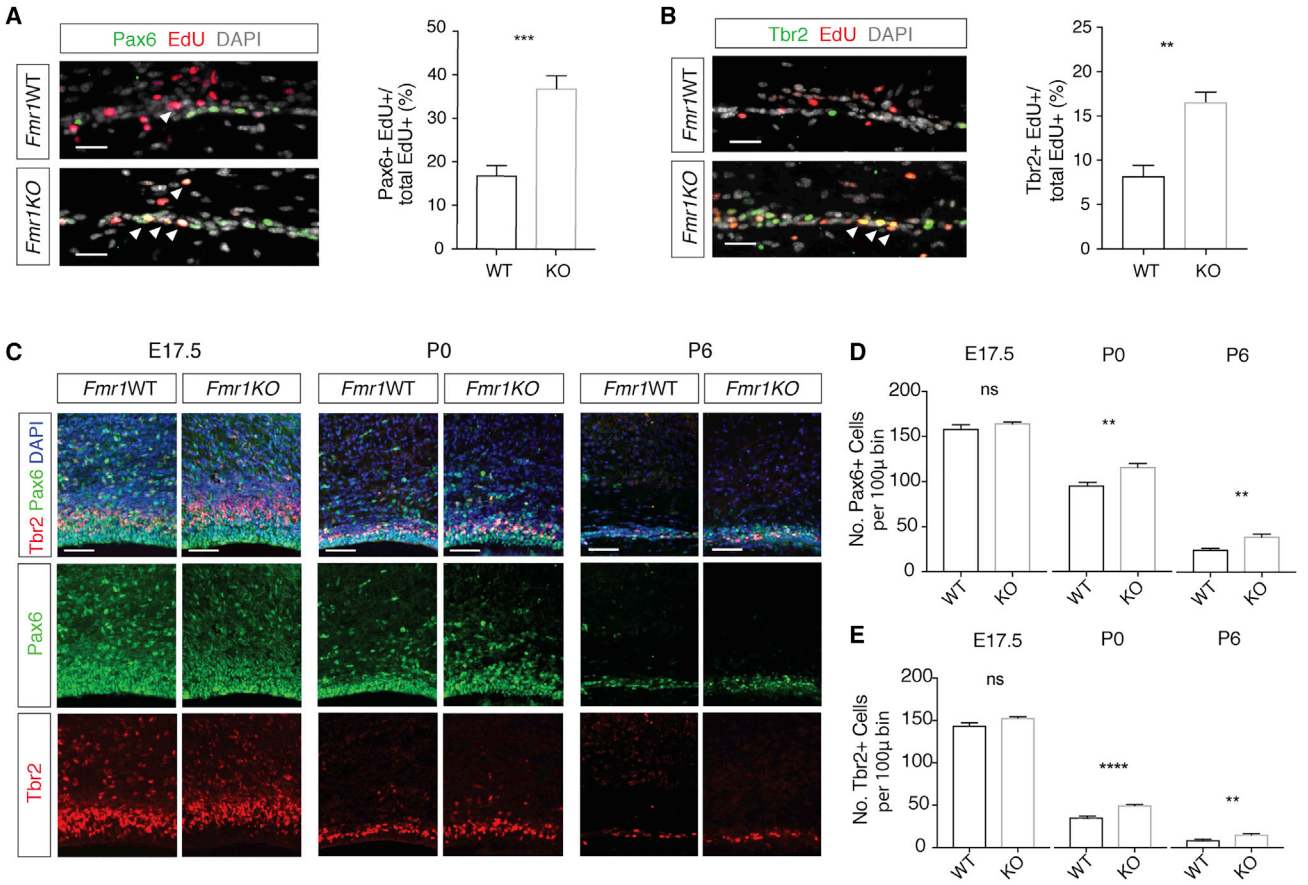

Figure 2. Genetic Deletion of *Fmr1* in Mice Results in Extended Maintenance of Proliferating Neural Progenitors in the Postnatal Mouse Cortex

(A) Immunostaining of Pax6 (green) and EdU (red) in P7 cortex from WT and *Fmr1*KO mice exposed to EdU (48 h). The number of $Pax6^+EdU^+$ cells, marked by arrowheads, is increased in KO cortex (***p = 0.0008; n = 5 WT, 4 KO mice). Scale bar, 25 μm. Data are presented as mean + SEM.

(B) Immunostaining of Tbr2 (green) and EdU (red) in P7 cortex from WT and *Fmr1*KO mice exposed to EdU (48 h). The number of $Tbr2^+EdU^+$ cells, marked by arrowheads, is increased in KO cortex (**p = 0.0018; n = 5 WT, 4 KO mice). Scale bar, 25 μm. Data are presented as mean + SEM.

(C) Immunostaining of Pax6 (green) and Tbr2 (red) in WT and *Frm1*KO cortex at E17.5, P0, and P6. Scale bar, 50 μm.

(D and E) $Pax6^+$ (D) and $Tbr2^+$ (E) cells are increased in *Fmr1*KO cortex: E17.5, $Pax6^+$ (p = 0.1996; n = 3 WT, 4 KO mice) and $Tbr2^+$ (p = 0.053; n = 3 WT, 4 KO mice); P0, $Pax6^+$ (**p = 0.0029; n = 7 WT, 7 KO mice) and $Tbr2^+$ (****p < 0.0001; n = 7 WT, 7 KO mice); P6, $Pax6^+$ (**p = 0.0058; n = 5WT, 6KO mice) and $Tbr2^+$ (**p = 0.0059; n = 5 WT, 6 KO mice). Data are presented as mean + SEM.

2015; Noor et al., 2010). We focused on six of the m^6A-modified, differentially expressed Notch- and Hedgehog-related mRNAs (*Ptch1*, *Dll1*, *Dlg5*, *Fat4*, *Gpr161*, and *Spop),* all of which are also validated FMRP targets (Ascano et al., 2012). We quantified the levels of these six targets in WT and *Fmr1*KO NPCs by qRT-PCR. Each mRNA showed increased nuclear retention in *Fmr1*KO NPCs (Figure 3I), suggesting a critical role for FMRP in the nuclear export of these methylated target mRNAs. None of these mRNAs showed increased whole-cell levels, indicating that the increase in nuclear levels was not caused by increased general transcription (Figure S3E). We next tested the effect of the loss of m^6A on the nuclear levels of these mRNAs in *Mettl14*cKO NPCs. The elevated nuclear retention of the FMRP target mRNAs observed in *Fmr1*KO NPCs was largely phenocopied in *Mettl14*cKO NPCs (Figure 3J), suggesting a nuclear export mechanism that requires both FMRP and m^6A.

FMRP Mediates the Nuclear Export of m^6A-Tagged Target mRNAs through CRM1

Our results indicate that FMRP can read m^6A and that loss of either *Fmr1* or m^6A results in the reduced nuclear export of methylated FMRP target mRNAs. Nuclear export of mRNA has been shown to be a critical mechanism regulating gene expression (Prasanth et al., 2005; Wegener and Muller-McNicoll, 2018). Therefore, nuclear export defects in *Mettl14cKO* NPCs may indicate the altered protein expression of methylated FMRP targets. Western blot analysis revealed a significant reduction in PTCH1 and DLL1 protein levels in *Mettl14cKO* NPCs compared to WT (Figures 4A and 4B). This finding further supports the functional importance of FMRP-m^6A-mediated nuclear export of mRNA in neural differentiation.

mRNAs can be exported from the nucleus through either NXF1 or CRM1 (Hutten and Kehlenbach, 2007). CRM1-dependent

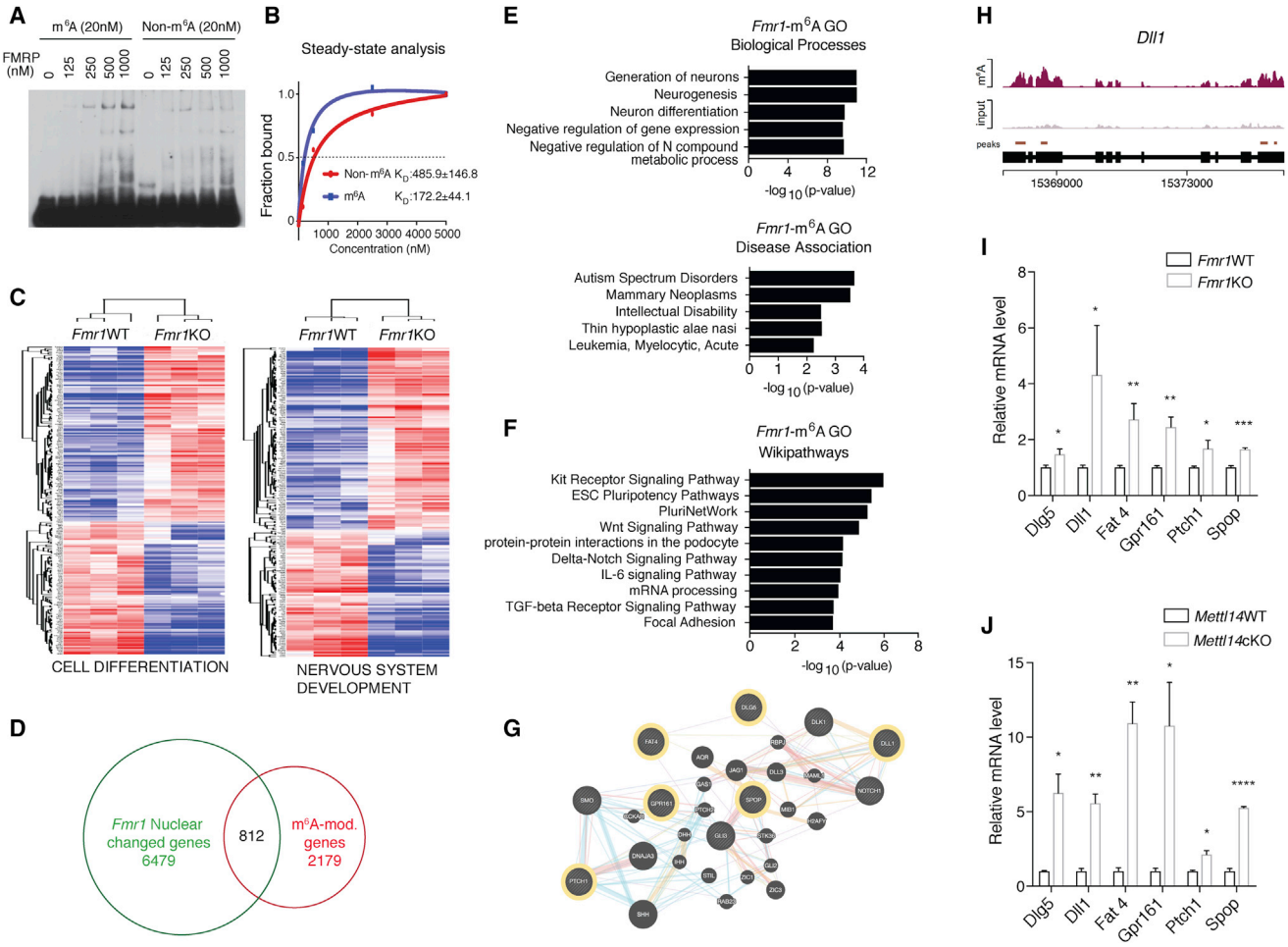

Figure 3. FMRP Preferentially Binds m^{6}A-Modified RNAs to Promote Their Nuclear Export in Regulating Neural Differentiation

(A) EMSA comparing FMRP binding to non-methylated (left) or methylated (right) RNA.

(B) Steady-state analysis of FMRP binding to methylated or non-methylated RNA using bio-layer interferometry. Results are averaged from three independent experiments.

(C) Heatmaps comparing WT and *Fmr1*KO NPC nuclear expression of genes related to cell differentiation (left) and nervous system development (right).

(D) Venn diagram showing RNAs that are m^{6}A modified and differentially expressed in *Fmr1*KO nucleus.

(E) Gene Ontology (GO) analysis of RNAs that are both differentially expressed in *Fmr1*KO nucleus and m^{6}A modified. Biological processes (top) and disease associations (bottom) are shown.

(F) Pathway analysis of RNAs that are both differentially expressed in *Fmr1KO* nucleus and m^{6}A modified.

(G) Gene interaction network of Hedgehog- and Notch-related signaling components and their cross-talk. m^{6}A-tagged FMRP targets are outlined in yellow.

(H) Coverage plot of m^{6}A modification of *Dll1* mRNA.

(I) RNAs of Hedgehog- and Notch-related components are retained in *Fmr1*KO nucleus quantified by qRT-PCR: *Dlg5* (*p = 0.0324), *Dll1* (*p = 0.0433), *Fat4* (**p = 0.0065), *Gpr161* (**p = 0.0020), *Ptch1* (*p = 0.0262), and *Spop* (***p = 0.0006); n = 5 WT, 3 KO biological replicates. Normalization is to *U1*. Data are presented as mean + SEM.

(J) RNAs of Hedgehog- and Notch-related components are retained in *Mettl14*cKO nucleus quantified by qRT-PCR: *Dlg5* (*p = 0.0180), *Dll1* (**p = 0.0016), *Fat4* (**p = 0.0021), *Gpr161* (*p = 0.0361), *Ptch1* (*p = 0.0164), and *Spop* (****p < 0.0001); n = 3 WT, 4 cKO biological replicates. Normalization is to *U1*. Data are presented as mean + SEM.

export is selective, requiring that target mRNAs first bind a CRM1-interacting RNA-binding protein. We identified specific CRM1-FMRP interaction by co-immunoprecipitation (Figure 4C). We also found nuclear accumulation of FMRP following CRM1 inhibition by leptomycin B (LMB) (Figures 4D, 4E, and S4A), suggesting that FMRP is exported from the nucleus through a CRM1-mediated mechanism. To determine whether m^{6}A-tagged FMRP target mRNAs related to Notch and Hedgehog signaling are exported through CRM1, we tested the nuclear levels of these mRNAs in LMB-treated NPCs. Following CRM1 inhibition, there was an increase in the nuclear levels of a majority of these targets (Figure 4F), suggesting that nuclear export of m^{6}A-tagged FMRP target mRNAs is mediated through CRM1. To determine the role of m^{6}A in this process, we performed RNA immunoprecipitation (RIP) of CRM1 in WT and *Mettl14*cKO NPCs, followed by quantification using qRT-PCR. There was a

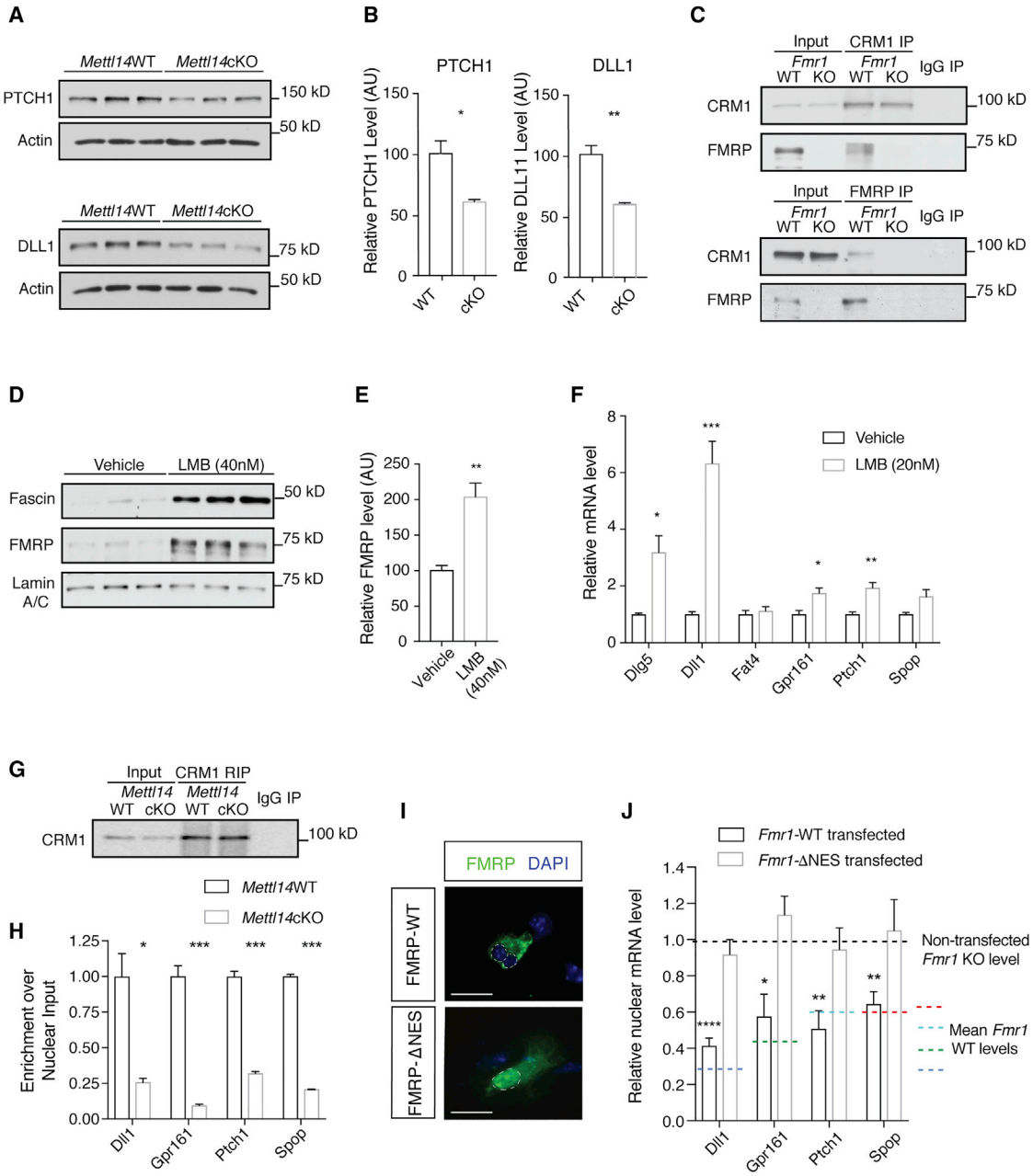

Figure 4. FMRP Mediates the Nuclear Export of m^{6}A-Tagged FMRP Target mRNAs through CRM1

(A) Western blot of PTCH1 and DLL1 in WT and *Mettl14*cKO NPC whole-cell lysates.

(B) PTCH1 (*p = 0.0178; n = 3 WT, 3 cKO biological replicates) and DLL1 (**p = 0.0045; n = 3 WT, 3 cKO biological replicates) protein levels are significantly decreased in *Mettl14*cKO NPCs. Data are presented as mean + SEM.

(C) Immunoprecipitation of CRM1 (top) or FMRP (bottom) co-precipitates FMRP or CRM1, respectively, in the WT mouse cortex.

(D) Western blot of CRM1 inhibition by LMB in WT NPC nuclear fractions. Lamin A-C serves as loading control and fascin as a positive control.

(E) The nuclear FMRP level is elevated in WT NPCs following LMB treatment (40 nM) (**p = 0.0069; n = 3 biological replicates). Data are presented as mean + SEM.

(F) Notch- and Hedgehog-related RNAs show nuclear retention in WT NPCs following LMB treatment (20 nM) quantified by qRT-PCR: *Dlg5* (*p = 0.0170), *Dll1* (***p = 0.0006), *Fat4* (p = 0.5815), *Gpr161* (*p = 0.0154), *Ptch1* (**p = 0.0048), and *Spop* (p = 0.0518); n = 4 vehicle, 6 LMB biological replicates. Normalization is to *Snora3*. Data are presented as mean + SEM.

(G) CRM1 RIP from WT or *Mettl14*cKO NPCs.

(H) CRM1 binding to Notch- and Hedgehog-related RNAs is reduced in *Mettl14*cKO NPCs quantified by qRT-PCR: *Dll1* (**p = 0.01), Gpr161 (***p = 0.00029), *Ptch1* (***p = 0.0002), and *Spop* (****p < 0.0001); n = 3 biological replicates. Normalization is to *U1*. Data are presented as mean + SEM.

(legend continued on next page)

significant reduction in CRM1 binding to FMRP target mRNAs in *Mettl14*cKO RIP samples (Figures 4G and 4H), suggesting that RNA methylation is required for CRM1 binding to m^{6}A-modified FMRP target mRNAs and their nuclear export. To further establish the functional link between FMRP and the nuclear export of m^{6}A-tagged target mRNAs, we reintroduced either WT *Fmr1* or the NES-lacking *Fmr1*ΔNES (Figure 4I) into *Fmr1*KO NPCs and assessed the levels of methylated FMRP target mRNAs by qRT-PCR. While the expression of WT FMRP significantly mitigated the nuclear retention of the methylated FMRP target mRNAs, expression of the nuclear-restricted FMRPΔNES produced no rescue effect (Figure 4J). These data demonstrate a critical role for FMRP in mediating the nuclear export of m^{6}A-tagged target mRNAs to regulate neural differentiation.

DISCUSSION

RNA methylation on N^6-adenosine is emerging as a vital mechanism regulating RNA metabolism and function (Dominissini et al., 2012; Meyer et al., 2012; Peer et al., 2017). Here, we report that FMRP regulates neural differentiation through m^{6}A-dependent mRNA nuclear export. We also elucidated the underlying mechanism by which FMRP preferentially binds m^{6}A-modified mRNAs and facilitates their nuclear export through CRM1 to regulate neural differentiation.

In *Fmr1*KO mice, we discovered delayed cell cycle progression and extended maintenance of proliferating neural progenitors into postnatal stages, which are also m^{6}A-dependent phenotypes found in methyltransferase *Mettl14*cKO mice that have no m^{6}A. These findings suggest a functional relation between FMRP and m^{6}A in neural differentiation. Our RNA-seq and m^{6}A-seq show that both *Mettl14cKO* and *Fmr1KO* lead to nuclear retention of m^{6}A-modified FMRP target mRNAs regulating neural differentiation, indicating that both m^{6}A methylation and FMRP are required for the nuclear export of target mRNAs. To establish the link between FMRP and m^{6}A, we first tested the role of m^{6}A in FMRP target mRNA nuclear export by CRM1 RIP in WT and *Mettl14*cKO NPCs. We found significantly reduced CRM1 binding to FMRP target mRNAs in *Mettl14*cKO NPCs that have no m^{6}A (Figures 4G and 4H). This finding highlights the importance of m^{6}A in CRM1-mediated nuclear export of FMRP targets. In addition, we also tested whether the reintroduction of FMRP could rescue the nuclear retention of m^{6}A-tagged FMRP target mRNAs, including components of Notch and Hedgehog signaling pathways that have well-established roles in regulating neural proliferation and differentiation. We found that only WT FMRP, not the NES-lacking and nuclear restricted FMRPΔNES, alleviated nuclear retention deficits in *Fmr1*KO NPCs (Figures 4I and 4J). Thus, FMRP is sufficient to drive the nuclear export of m^{6}A-tagged FMRP target mRNAs, and this mechanism requires the NES-nuclear export. Our findings establish a critical role for FMRP in regulating m^{6}A-dependent mRNA nuclear export during neural differentiation.

Recently, in a large-scale screen to establish a global m^{6}A interactome using mass spectrometry, FMRP was found to be one of more than 20 candidate proteins that may interact with an m^{6}A-modified probe of 4 GGACU repeats with higher affinity in cell lines (Edupuganti et al., 2017). However, a separate study found no preferential binding of FMRP to m^{6}A-modified RNA probes (Zhang et al., 2018), although specific enrichment of m^{6}A in FMRP targets was discovered. The discrepancy could be due to differences in experimental conditions, design of RNA probes, or the quality of purified FMRP protein used. We used full-length FMRP iso1 purified from Sf9 cells and probe RNA sequences from mouse *Dll1* mRNA containing both consensus FMRP-binding sites and RNA methylation motifs to show that FMRP preferentially binds to methylated RNA in both EMSA and bio-layer interferometry analysis. Our data establish the role of FMRP as an m^{6}A reader both *in vivo* and *in vitro*.

The nuclear export of mRNAs related to Notch and Hedgehog signaling was found in our study to require both FMRP and m^{6}A. Delta-like (Dll) binding to the Notch receptor drives the expression of *Hes1* to maintain stem cell pluripotency and suppress differentiation (Ishibashi et al., 1995). Notch has also been shown to cross-talk with additional pathways, including Hedgehog, to regulate neural stem cell proliferation and differentiation. Hedgehog-induced maintenance of stem cell pluripotency relies in part on the activation of Notch to balance proliferation with differentiation (Dave et al., 2011; Kong et al., 2015). We found increased nuclear retention of m^{6}A-modified FMRP targets related to Notch and Hedgehog pathways in both *Fmr1KO* and *Mettl14cKO* NPCs. Our findings suggest that a disruption in the balance between proliferation and differentiation regulated by FMRP-m^{6}A-dependent nuclear export may underlie the aberrant neural differentiation phenotypes observed in *Fmr1KO* and *Mettl14cKO* mice, eventually leading to defects in neuronal function.

We discovered the extended maintenance of neural progenitors into postnatal stages, accompanied by delayed cell cycle progression and neural differentiation in *Fmr1*KO mice. Cell cycle phase and duration are tightly coupled to neurogenic potential (McConnell and Kaznowski, 1991; Pilaz et al., 2016). Moreover, there is a strong association between neuronal birthdate and identity (Rakic, 1988). Therefore, the temporal aberrations in neural progenitor cell cycle and differentiation observed in *Fmr1*KO mice may influence cortical development by affecting neuron subtype specification, contributing to functional deficits in fragile X syndrome. Consistent with our observations, alterations of layer-specific neuron migration and localization have been found in *Fmr1*KO mice (La Fata et al., 2014; Tervonen et al., 2009). In addition, delayed cell cycle exit in *Fmr1*KO progenitors may deregulate the excitatory-inhibitory balance in the developing neural circuitry, as inhibitory interneuron integration into the cortex follows and depends upon pyramidal neuron differentiation and patterning

(I) Cytoplasmic localization of FMRP-WT and nuclear localization of FMRPΔNES in *Fmr1*KO NPCs. Scale bar, 20 μm.

(J) Nuclear retention of target mRNAs in *Fmr1*KO NPCs is rescued by the expression of WT (*Dll1* [****p < 0.0001], Gpr161 [*p = 0.026], *Ptch1* [**p = 0.008], and *Spop* [**p = 0.006]; n = 3 biological replicates) but not ΔNES *Fmr1* (*Dll1* [p = 0.372], *Gpr161* [p = 0.253], *Ptch1* [p = 0.672], *Spop* [p = 0.78]; n = 3 biological replicates). Data are presented as mean + SEM.

(Bartolini et al., 2013). Defects in these processes in *Fmr1*KO mice could drive the altered synaptic landscape that is characteristic of fragile X syndrome. Our study elucidates a mechanism by which FMRP reads and facilitates the nuclear export of m^{6}A-modified mRNAs to regulate neural differentiation, defects in which may contribute to functional deficits in fragile X syndrome.

STAR★METHODS

Detailed methods are provided in the online version of this paper and include the following:

- KEY RESOURCES TABLE
- LEAD CONTACT AND MATERIALS AVAILABILITY
- EXPERIMENTAL MODEL AND SUBJECT DETAILS
- METHOD DETAILS
  - Cell Culture
  - Immunohistochemistry
  - Flow Cytometry
  - Nuclear RNA Extraction and Quality Control
  - qRT-PCR
  - RNA Sequencing and Analysis
  - Immunoprecipitation
  - RNA Immunoprecipitation (RIP)
  - Electrophoretic Mobility Shift Assay (EMSA)
  - Bio-Layer Interferometry Analysis
  - Western Blot
  - Nucleofection of NPCs
- QUANTIFICATION AND STATISTICAL ANALYSIS
- DATA AND CODE AVAILABILITY

SUPPLEMENTAL INFORMATION

Supplemental Information can be found online at https://doi.org/10.1016/j.celrep.2019.06.072.

ACKNOWLEDGMENTS

This research was supported by grants from the NIH (R01NS094564 and R21NS106307 to Y.C.M.; R37NS047344, U19MH106434, and P01NS097206 to H. Song; RM1HG008935 to C.H.; and R01MH105128, R35NS097370, and U19AI131130 to G.-l.M.); the Simons Foundation Autism Research Initiative (SAFRI) to H. Song (575050); Cure SMA and The Hartwell Foundation (to Y.C.M.); and the Chicago Biomedical Consortium (to Y.C.M. and C.H.). C.V. was partially supported by an NSF predoctoral fellowship and NIH T32GM007445. We thank Dr. Stephanie Ceman for providing WT and ΔNES *Fmr1* constructs, Dr. Anis Contractor for providing *Fmr1* KO mice, and Dr. Xiaoxi Zhuang for sharing *Mettl14*$^{f/f}$ mice. We thank Dr. Tian Shao for technical assistance in validating anti-FMRP antibodies. The research reported in this manuscript was made possible in part by the services of the Keck Biophysics Facility and the NUSeq Core Facility, which is supported by the Northwestern University Center for Genetic Medicine, the Feinberg School of Medicine, and the Shared and Core Facilities of Northwestern University's Office for Research. C.H. is a Howard Hughes Medical Institute Investigator. Y.C.M. is the Ann Marie and Francis Klocke M.D. Research Scholar supported by the Joseph and Bessie Feinberg Foundation.

AUTHOR CONTRIBUTIONS

B.M.E. and Y.C.M. designed the experiments and contributed to most of the aspects of the study. C.V. provided *Mettl14*cKO NPCs and contributed to fluorescence-activated cell sorting (FACS) cell-cycle analysis. J.S. and Z.X. contributed to qRT-PCR analysis. S.A. contributed to EMSA binding assays and mouse husbandry. H. Shi contributed to the RNA sequencing analysis. N.M. prepared many mouse RNA samples. F.R.R. and G.-l.M. provided the *Dll1* m^{6}A coverage plot. Y.C.M., C.H., and H. Song initiated the project. B.M.E. and Y.C.M. wrote the manuscript. Y.C.M. managed the project.

DECLARATION OF INTERESTS

C.H. is a scientific founder and scientific advisory board member of Accent Therapeutics, Inc.

Received: November 8, 2018
Revised: April 9, 2019
Accepted: June 20, 2019
Published: July 23, 2019

REFERENCES

Ascano, M., Jr., Mukherjee, N., Bandaru, P., Miller, J.B., Nusbaum, J.D., Corcoran, D.L., Langlois, C., Munschauer, M., Dewell, S., Hafner, M., et al. (2012). FMRP targets distinct mRNA sequence elements to regulate protein expression. Nature *492*, 382–386.

Bartolini, G., Ciceri, G., and Marín, O. (2013). Integration of GABAergic interneurons into cortical cell assemblies: lessons from embryos and adults. Neuron *79*, 849–864.

Batista, P.J., Molinie, B., Wang, J., Qu, K., Zhang, J., Li, L., Bouley, D.M., Lujan, E., Haddad, B., Daneshvar, K., et al. (2014). m(6)A RNA modification controls cell fate transition in mammalian embryonic stem cells. Cell Stem Cell *15*, 707–719.

Castrén, M., Tervonen, T., Kärkkäinen, V., Heinonen, S., Castrén, E., Larsson, K., Bakker, C.E., Oostra, B.A., and Akerman, K. (2005). Altered differentiation of neural stem cells in fragile X syndrome. Proc. Natl. Acad. Sci. USA *102*, 17834–17839.

Chaudhry, A., Noor, A., Degagne, B., Baker, K., Bok, L.A., Brady, A.F., Chitayat, D., Chung, B.H., Cytrynbaum, C., Dyment, D., et al.; DDD Study (2015). Phenotypic spectrum associated with PTCHD1 deletions and truncating mutations includes intellectual disability and autism spectrum disorder. Clin. Genet. *88*, 224–233.

Chen, J., Bardes, E.E., Aronow, B.J., and Jegga, A.G. (2009). ToppGene Suite for gene list enrichment analysis and candidate gene prioritization. Nucleic Acids Res *37*, W305–W311.

Darnell, J.C., Van Driesche, S.J., Zhang, C., Hung, K.Y., Mele, A., Fraser, C.E., Stone, E.F., Chen, C., Fak, J.J., Chi, S.W., et al. (2011). FMRP stalls ribosomal translocation on mRNAs linked to synaptic function and autism. Cell *146*, 247–261.

Dave, R.K., Ellis, T., Toumpas, M.C., Robson, J.P., Julian, E., Adolphe, C., Bartlett, P.F., Cooper, H.M., Reynolds, B.A., and Wainwright, B.J. (2011). Sonic hedgehog and notch signaling can cooperate to regulate neurogenic divisions of neocortical progenitors. PLoS One *6*, e14680.

Dominissini, D., Moshitch-Moshkovitz, S., Schwartz, S., Salmon-Divon, M., Ungar, L., Osenberg, S., Cesarkas, K., Jacob-Hirsch, J., Amariglio, N., Kupiec, M., et al. (2012). Topology of the human and mouse m6A RNA methylomes revealed by m6A-seq. Nature *485*, 201–206.

Du, H., Zhao, Y., He, J., Zhang, Y., Xi, H., Liu, M., Ma, J., and Wu, L. (2016). YTHDF2 destabilizes m(6)A-containing RNA through direct recruitment of the CCR4-NOT deadenylase complex. Nat. Commun. *7*, 12626.

Dutch-Belgian Fragile X Consortium (1994). Fmr1 knockout mice: a model to study fragile X mental retardation. Cell *78*, 23–33.

Dwyer, N.D., Chen, B., Chou, S.J., Hippenmeyer, S., Nguyen, L., and Ghashghaei, H.T. (2016). Neural Stem Cells to Cerebral Cortex: Emerging Mechanisms Regulating Progenitor Behavior and Productivity. J. Neurosci. *36*, 11394–11401.

Eberhart, D.E., Malter, H.E., Feng, Y., and Warren, S.T. (1996). The fragile X mental retardation protein is a ribonucleoprotein containing both nuclear localization and nuclear export signals. Hum. Mol. Genet. *5*, 1083–1091.

Edupuganti, R.R., Geiger, S., Lindeboom, R.G.H., Shi, H., Hsu, P.J., Lu, Z., Wang, S.Y., Baltissen, M.P.A., Jansen, P.W.T.C., Rossa, M., et al. (2017). N^6-methyladenosine (m^6A) recruits and repels proteins to regulate mRNA homeostasis. Nat. Struct. Mol. Biol. *24*, 870–878.

Engel, M., Eggert, C., Kaplick, P.M., Eder, M., Roh, S., Tietze, L., Namendorf, C., Arloth, J., Weber, P., Rex-Haffner, M., et al. (2018). The Role of m(6)A/m-RNA Methylation in Stress Response Regulation. Neuron *99*, 389–403.e9.

Fu, Y., Dominissini, D., Rechavi, G., and He, C. (2014). Gene expression regulation mediated through reversible m^6A RNA methylation. Nat. Rev. Genet. *15*, 293–306.

Fustin, J.M., Doi, M., Yamaguchi, Y., Hida, H., Nishimura, S., Yoshida, M., Isagawa, T., Morioka, M.S., Kakeya, H., Manabe, I., and Okamura, H. (2013). RNA-methylation-dependent RNA processing controls the speed of the circadian clock. Cell *155*, 793–806.

Geula, S., Moshitch-Moshkovitz, S., Dominissini, D., Mansour, A.A., Kol, N., Salmon-Divon, M., Hershkovitz, V., Peer, E., Mor, N., Manor, Y.S., et al. (2015). Stem cells. m6A mRNA methylation facilitates resolution of naïve pluripotency toward differentiation. Science *347*, 1002–1006.

Herwig, R., Hardt, C., Lienhard, M., and Kamburov, A. (2016). Analyzing and interpreting genome data at the network level with ConsensusPathDB. Nat. Protoc *11*, 1889–1907.

Hutten, S., and Kehlenbach, R.H. (2007). CRM1-mediated nuclear export: to the pore and beyond. Trends Cell Biol. *17*, 193–201.

Ishibashi, M., Ang, S.L., Shiota, K., Nakanishi, S., Kageyama, R., and Guillemot, F. (1995). Targeted disruption of mammalian hairy and enhancer of split homolog-1 (HES-1) leads to up-regulation of neural helix-loop-helix factors, premature neurogenesis, and severe neural tube defects. Genes Dev. *9*, 3136–3148.

Jia, G., Fu, Y., Zhao, X., Dai, Q., Zheng, G., Yang, Y., Yi, C., Lindahl, T., Pan, T., Yang, Y.G., and He, C. (2011). N6-methyladenosine in nuclear RNA is a major substrate of the obesity-associated FTO. Nat. Chem. Biol. *7*, 885–887.

Ke, S., Pandya-Jones, A., Saito, Y., Fak, J.J., Vågbø, C.B., Geula, S., Hanna, J.H., Black, D.L., Darnell, J.E., Jr., and Darnell, R.B. (2017). m^6A mRNA modifications are deposited in nascent pre-mRNA and are not required for splicing but do specify cytoplasmic turnover. Genes Dev. *31*, 990–1006.

Kim, M., Bellini, M., and Ceman, S. (2009). Fragile X mental retardation protein FMRP binds mRNAs in the nucleus. Mol. Cell. Biol. *29*, 214–228.

Kong, J.H., Yang, L., Dessaud, E., Chuang, K., Moore, D.M., Rohatgi, R., Briscoe, J., and Novitch, B.G. (2015). Notch activity modulates the responsiveness of neural progenitors to sonic hedgehog signaling. Dev. Cell *33*, 373–387.

Koranda, J.L., Dore, L., Shi, H., Patel, M.J., Vaasjo, L.O., Rao, M.N., Chen, K., Lu, Z., Yi, Y., Chi, W., et al. (2018). Mettl14 Is Essential for Epitranscriptomic Regulation of Striatal Function and Learning. Neuron *99*, 283–292.e5.

La Fata, G., Gärtner, A., Domínguez-Iturza, N., Dresselaers, T., Dawitz, J., Poorthuis, R.B., Averna, M., Himmelreich, U., Meredith, R.M., Achsel, T., et al. (2014). FMRP regulates multipolar to bipolar transition affecting neuronal migration and cortical circuitry. Nat. Neurosci. *17*, 1693–1700.

Lin, S., Choe, J., Du, P., Triboulet, R., and Gregory, R.I. (2016). The m(6)A Methyltransferase METTL3 Promotes Translation in Human Cancer Cells. Mol. Cell *62*, 335–345.

Liu, J., Yue, Y., Han, D., Wang, X., Fu, Y., Zhang, L., Jia, G., Yu, M., Lu, Z., Deng, X., et al. (2014). A METTL3-METTL14 complex mediates mammalian nuclear RNA N6-adenosine methylation. Nat. Chem. Biol. *10*, 93–95.

McConnell, S.K., and Kaznowski, C.E. (1991). Cell cycle dependence of laminar determination in developing neocortex. Science *254*, 282–285.

Meyer, K.D., Saletore, Y., Zumbo, P., Elemento, O., Mason, C.E., and Jaffrey, S.R. (2012). Comprehensive analysis of mRNA methylation reveals enrichment in 3′UTRs and near stop codons. Cell *149*, 1635–1646.

Meyer, K.D., Patil, D.P., Zhou, J., Zinoviev, A., Skabkin, M.A., Elemento, O., Pestova, T.V., Qian, S.B., and Jaffrey, S.R. (2015). 5′ UTR m(6)A Promotes Cap-Independent Translation. Cell *163*, 999–1010.

Noor, A., Whibley, A., Marshall, C.R., Gianakopoulos, P.J., Piton, A., Carson, A.R., Orlic-Milacic, M., Lionel, A.C., Sato, D., Pinto, D., et al.; Autism Genome Project Consortium (2010). Disruption at the PTCHD1 Locus on Xp22.11 in Autism spectrum disorder and intellectual disability. Sci. Transl. Med. *2*, 49ra68.

Peer, E., Rechavi, G., and Dominissini, D. (2017). Epitranscriptomics: regulation of mRNA metabolism through modifications. Curr. Opin. Chem. Biol. *41*, 93–98.

Pilaz, L.J., McMahon, J.J., Miller, E.E., Lennox, A.L., Suzuki, A., Salmon, E., and Silver, D.L. (2016). Prolonged Mitosis of Neural Progenitors Alters Cell Fate in the Developing Brain. Neuron *89*, 83–99.

Prasanth, K.V., Prasanth, S.G., Xuan, Z., Hearn, S., Freier, S.M., Bennett, C.F., Zhang, M.Q., and Spector, D.L. (2005). Regulating gene expression through RNA nuclear retention. Cell *123*, 249–263.

Rakic, P. (1988). Specification of cerebral cortical areas. Science *241*, 170–176.

Richter, J.D., Bassell, G.J., and Klann, E. (2015). Dysregulation and restoration of translational homeostasis in fragile X syndrome. Nat. Rev. Neurosci. *16*, 595–605.

Roundtree, I.A., Luo, G.Z., Zhang, Z., Wang, X., Zhou, T., Cui, Y., Sha, J., Huang, X., Guerrero, L., Xie, P., et al. (2017). YTHDC1 mediates nuclear export of N^6-methyladenosine methylated mRNAs. eLife *6*, e31311.

Saffary, R., and Xie, Z. (2011). FMRP regulates the transition from radial glial cells to intermediate progenitor cells during neocortical development. J. Neurosci. *31*, 1427–1439.

Shen, M., Wang, F., Li, M., Sah, N., Stockton, M.E., Tidei, J.J., Gao, Y., Korabelnikov, T., Kannan, S., Vevea, J.D., et al. (2019). Reduced mitochondrial fusion and Huntingtin levels contribute to impaired dendritic maturation and behavioral deficits in Fmr1-mutant mice. Nat. Neurosci. *22*, 386–400.

Solecki, D.J., Model, L., Gaetz, J., Kapoor, T.M., and Hatten, M.E. (2004). Par6alpha signaling controls glial-guided neuronal migration. Nat. Neurosci. *7*, 1195–1203.

Tervonen, T.A., Louhivuori, V., Sun, X., Hokkanen, M.E., Kratochwil, C.F., Zebryk, P., Castrén, E., and Castrén, M.L. (2009). Aberrant differentiation of glutamatergic cells in neocortex of mouse model for fragile X syndrome. Neurobiol. Dis. *33*, 250–259.

Wang, X., Lu, Z., Gomez, A., Hon, G.C., Yue, Y., Han, D., Fu, Y., Parisien, M., Dai, Q., Jia, G., et al. (2014). N6-methyladenosine-dependent regulation of messenger RNA stability. Nature *505*, 117–120.

Wang, X., Zhao, B.S., Roundtree, I.A., Lu, Z., Han, D., Ma, H., Weng, X., Chen, K., Shi, H., and He, C. (2015). N(6)-methyladenosine Modulates Messenger RNA Translation Efficiency. Cell *161*, 1388–1399.

Wang, Y., Li, Y., Yue, M., Wang, J., Kumar, S., Wechsler-Reya, R.J., Zhang, Z., Ogawa, Y., Kellis, M., Duester, G., and Zhao, J.C. (2018). N^6-methyladenosine RNA modification regulates embryonic neural stem cell self-renewal through histone modifications. Nat. Neurosci. *21*, 195–206.

Warde-Farley, D., Donaldson, S.L., Comes, O., Zuberi, K., Badrawi, R., Chao, P., Franz, M., Grouios, C., Kazi, F., Lopes, C.T., et al. (2010). The GeneMANIA production server: biological network integration for gene prioritization and predicting gene function. Nucleic Acids Res *38*, W214–W220.

Wegener, M., and Muller-McNicoll, M. (2018). Nuclear retention of mRNAs - quality control, gene regulation and human disease. Semin. Cell Dev. Biol. *79*, 131–142.

Wei, J., Liu, F., Lu, Z., Fei, Q., Ai, Y., He, P.C., Shi, H., Cui, X., Su, R., Klungland, A., et al. (2018). Differential m(6)A, m(6)Am, and m(1)A Demethylation Mediated by FTO in the Cell Nucleus and Cytoplasm. Mol. Cell *71*, 973–985.e5.

Xu, C., Wang, X., Liu, K., Roundtree, I.A., Tempel, W., Li, Y., Lu, Z., He, C., and Min, J. (2014). Structural basis for selective binding of m6A RNA by the YTHDC1 YTH domain. Nat. Chem. Biol. *10*, 927–929.

Yoon, K.J., Ringeling, F.R., Vissers, C., Jacob, F., Pokrass, M., Jimenez-Cyrus, D., Su, Y., Kim, N.S., Zhu, Y., Zheng, L., et al. (2017). Temporal Control of Mammalian Cortical Neurogenesis by m(6)A Methylation. Cell *171*, 877–889.e17.

Zhang, F., Kang, Y., Wang, M., Li, Y., Xu, T., Yang, W., Song, H., Wu, H., Shu, Q., and Jin, P. (2018). Fragile X mental retardation protein modulates the stability of its m6A-marked messenger RNA targets. Hum. Mol. Genet. *27*, 3936–3950.

STAR★METHODS

KEY RESOURCES TABLE

REAGENT or RESOURCE	SOURCE	IDENTIFIER
Antibodies		
Mouse monoclonal anti-Pax6 (clone 018-1330)	BD Biosciences	Cat# 561462; RRID:AB_10715442
Rabbit polyclonal anti-Tbr2	Abcam	Cat# ab23345; RRID:AB_778267
Rabbit polyclonal anti-GFAP	DAKO	Cat# Z0334; RRID:AB_10013382
Rat monoclonal anti-Ki-67	DAKO	Cat# M7249; RRID:AB_2250503
Rabbit polyclonal anti-phospho Histone H3	CST	Cat# 9701; RRID:AB_331535
Rabbit polyclonal anti-FMRP	CST	Cat# 4317S; RRID:AB_1903978
Rabbit polyclonal anti-CRM1	Bethyl Labs	Cat# A300-469A; RRID:AB_451004
Rabbit polyclonal anti-Lamin A/C	CST	Cat# 2032; RRID:AB_2136278
Mouse monoclonal anti-Beta-tubulin	Fisher	Cat# A2228; RRID:AB_476697
Mouse monoclonal anti-Fascin	SCBT	Cat# sc-21743; RRID:AB_627580
Rabbit polyclonal anti-PTCH1	Proetintech	Cat# 17520-1-AP; RRID:AB_2176561
Rat monoclonal anti-DLL1	Millipore/Sigma	Cat# MABN2284
Peroxidase AffiniPure Goat Anti-Rabbit IgG (H+L)	Jackson Immunoresearch	Cat# 111035003
Peroxidase AffiniPure Goat Anti-Mouse IgG (H+L)	Jackson Immunoresearch	Cat# 115035003
Cy3 AffiniPure Donkey Anti-Rabbit IgG (H+L)	Jackson Immunoresearch	Cat# 711165152
Cy2 AffiniPure Donkey Anti-Mouse IgG (H+L)	Jackson Immunoresearch	Cat# 715225150
Cy2 AffiniPure Donkey Anti-Rat IgG (H+L)	Jackson Immunoresearch	Cat# 712225153
Chemicals, Peptides, and Recombinant Proteins		
FMRP Recombinant Protein (isoform 1)	AB Clonal	N/A
EdU (5-ethynyl-2-deoxyuridine)	Invitrogen	Cat# A10044
Paraformaldehyde	Sigma	Cat# P6148-1kg CAS 30525-89-4
PFA, 16% ultrapure EM grade	Polysciences	Cat# 18814-20
Target Retrieval Solution	Agilent/DAKO	Cat# S1699
7-AAD	Thermo Fisher Scientific	Cat# A1310
StemPro Accutase	Fisher Scientific	Cat# A1110501
SUPER Rase In RNase inhibitor	Fisher Scientific/Ambion	Cat# AM2696
Matrigel	Corning	Cat# #354234
DMEM-F12	Fisher Scientific/GIBCO	Cat# 11320-033
N-2 Supplement	Fisher Scientific/GIBCO	Cat# 17502048
B27 serum free supplement	Fisher Scientific/GIBCO	Cat# 17504-044
Glutamax	Fisher Scientific/GIBCO	Cat# 35050061
Recombinant Human bFGF	PeproTech	Cat# 100-18B
recombinant murine EGF	PeproTech	Cat# 315-09
Heparin	J.T. Baker/Avantor	Cat # M916-00
Complete, Mini, EDTA-free Protease Inhibitor Cocktail	Roche	Cat# 11836170001
Proteinase K	VWR	Cat# 97062-670
Normal Goat Serum	Jackson Immunoresearch	Cat# 005000121
Normal Donkey Serum	Jackson Immunoresearch	Cat# 017000121
Bovine Serum Albumin, Fraction V, Heat Shock Treated	Fisher Scientific	Cat# BP1600100
Leptomycin B	SCBT	Cat# sc-358688, CAS 87081-35-4
TRIzol	Invitrogen	Cat# 15-596-026

(*Continued on next page*)

Continued		
REAGENT or RESOURCE	SOURCE	IDENTIFIER
Critical Commercial Assays		
Click-iT Plus EdU Alexa Fluor 647 Flow Cytometry Assay Kit	Invitrogen	Cat# C10635
Click-iT Plus EdU Alexa Fluor 647 Imaging Kit	Invitrogen	Cat# C10640
Chemiluminescent Nucleic Acid Detection Module	Fisher Scientific/Pierce	Cat# PI89880
NE-PER Nuclear and Cytoplasmic Extraction Kit	Thermo Fisher Scientific	Cat# PI78835
QuantaBio PerfeCTa SYBR® Green SuperMix with Low ROX	VWR	Cat# 101414-162
QuantaBio qScript cDNA SuperMix	VWR	Cat# 101414-106
Quant-iT RNA HS Assay Kit	Invitrogen	Cat# Q32852
TruSeq RNA Seq Library Prep Kit	Illumina	Cat# RS-122-2001
Deposited Data		
Fmr1 Nuclear Fraction RNA Seq data	This paper	GSE121809
Experimental Models: Cell Lines		
Nestin-Cre$^{+/+}$; *Mettl14*$^{f/f}$ –derived NPCs	Yoon et al., 2017	N/A
Experimental Models: Organisms/Strains		
B6.129P2-*Fmr1*^{tm1Cgr}/J	Jackson Laboratory	RRID:IMSR_JAX:003025
Oligonucleotides		
m^{6}A *Dll1* oligo: 5′-GAACACCAACAAGAAGGCGGX CUUUCACGGGG m^{6}ACCAUGGAGCCGA-3′	This paper	N/A
Non-m^{6}A *Dll1* oligo: 5′-GAACACCAACAAGAAGGC GGXCUUUCACGGGGACCAUGGAGCCGA-3′	This paper	N/A
m^{6}A short oligo: 5′-CGUGG m^{6}ACUGGCU-3′	This paper	N/A
Non-m^{6}A short oligo: 5′-CGUGGACUGGCU-3′	This paper	N/A
m^{6}A mutated oligo: 5′-GAUAC m^{6}AGAGAAG-3′	This paper	N/A
Non-m^{6}A mutated oligo: 5′-GAUACAGAGAAG-3′	This paper	N/A
Primers for qPCR, see Table S1	This paper	N/A
Software and Algorithms		
FlowJo	FlowJo, LLC	RRID:SCR_008520, https://www.flowjo.com
TOPPGENE	Chen et al., 2009	RRID:SCR_005726, https://toppgene.cchmc.org
GeneMANIA	Warde-Farley et al., 2010	RRID:SCR_005709, http://genemania.org
Consensus Path-DB	Herwig et al., 2016	http://cpdb.molgen.mpg.de
R	R Project for Statistical Computing	RRID:SCR_001905, https://www.r-project.org
MATLAB	MathWorks	RRID:SCR_001622,https://www.mathworks.com/products/matlab.html
Prism7	GraphPad	SCR_002798; https://www.graphpad.com
Other		
Protein A Dynabeads	Invitrogen	Cat# 10-001-D
Protein A/G PLUS-Agarose	SCBT	Cat# sc-2003; RRID:AB_10201400
Kinematica Polytron PT 1200E Electric Homogenizer	Fisher Scientific	Cat# 05-400-261
5 Prime Phase Lock Gel Heavy 2 ml	VWR	Cat #10847-802
BioDYNE B nylon membrane	Fisher Scientific/Pierce	Cat #77016
Dip and Read Anti-Penta-HIS (HIS1K) Biosensors	Forte Bio	Cat #18-5120

LEAD CONTACT AND MATERIALS AVAILABILITY

Further information and requests for resources and reagents should be directed to and will be fulfilled by the Lead Contact, Yongchao C. Ma (ma@northwestern.edu).

EXPERIMENTAL MODEL AND SUBJECT DETAILS

All animal experiments conducted within this study have been approved by the Institutional Animal Care and Use Committee (Protocol #IS6359), and performed in accordance with federal regulations governing the use of animals in laboratory research. All animals were maintained in standard housing conditions with 12-hour light/dark cycle and food and water available *ad libitum*. *Fmr1* mice (*B6.129P2-Fmr1*$^{tm1Cgr/J}$ Jackson Laboratory #003025), originally generated by the Dutch-Belgian Fragile X Consortium (1994), were obtained through Dr. Anis Contractor from Dr. David Nelson's laboratory, where the original knockout line was backcrossed onto C57/BL6 background. Heterozygous *Fmr1* female mice were bred with C57/BL6 males to yield wild-type and knockout littermates for all FMRP experiments at indicated time points (E17.5, P0, P5, or P7), or utilized for generation of neural precursor cells (NPCs) at E13.5. Because *Fmr1* is an X-linked gene, only males were used for knockout analysis with the mating scheme described.

METHOD DETAILS

Cell Culture

Dorsal forebrains from timed-pregnant E13.5 mouse embryos were digested with Accutase (Fisher) to yield dissociated cortical neural precursor cells (NPCs) for culture. NPCs were carried on plates coated with Matrigel (Corning) at 80 μg/ml and maintained in DMEM-F12 medium (GIBCO) supplemented with B27 (GIBCO), N2 (GIBCO), and Glutamax (GIBCO). A growth factor cocktail containing EGF (PeproTech) (20ng/ml) and basic FGF (PeproTech) (20ng/ml) in Heparin (5 μg/ml) was added to the medium fresh. Cells were carried at densities not exceeding 80%, and all experiments were performed on density- and passage-matched NPC cultures. Cells were incubated in standard conditions: 37°C with 5% CO_2. Multiple lines of NPCs were generated from independent litters of *Fmr1* wild-type and knockout embryos.

Immunohistochemistry

Brains harvested from embryonic stages were fixed in fresh 4% PFA (Sigma) for six hours at 4°C, then washed extensively in PBS prior to embedding. Postnatal mice were subjected to transcardial perfusion with PBS, then PFA before brains were harvested and fixed in fresh 4% PFA for either six hours (P0), or overnight (P5, P7). Coronal sections (18 μm) were prepared using a Leica CM 3050S cryostat. Slides were baked at 65°C for two hours. For antigen retrieval, slides were submerged in Antigen Unmasking Solution (DAKO) at 95°C for twenty minutes, then rehydrated in PBS for five minutes. Sections were blocked for one hour at room temperature in 0.01% PBS-TritonX containing 3% BSA and 5% goat and donkey serum. Sections were incubated with primary antibodies overnight, and secondary antibodies for one hour at room temperature. All antibodies were diluted in blocking solution as follows: rat anti-Ki-67 (DAKO, 1:10), rabbit anti-GFAP (DAKO, 1:200), rabbit anti-phospho-Histone H3 (CST, 1:400), rabbit anti-Tbr2 (Abcam, 1:400), and mouse anti-Pax6 (BD Biosciences, 1:400). For embryonic EdU experiments, timed-pregnant dames were injected with EdU at a concentration of 150mg/kg for the indicated durations (2 hours or 24 hours). For postnatal EdU experiments, pups were given an injection of EdU at a concentration of 75mg/kg for the indicated duration (forty-eight hours). For EdU detection, the Click-iT Plus EdU Alexa Fluor 647 Imaging Kit (Invitrogen) was used according to manufacturer's protocol. Images were acquired on a Leica DM 2500 epifluorescence microscope outfitted with a RETIGA 4000R camera (Q-Imaging). Cell counts represent the total number of labeled cells (as indicated) within 100 μm bins.

Flow Cytometry

NPCs were exposed to EdU for a duration of thirty minutes, and then either fixed immediately or incubated for five hours and then fixed, and incorporation was detected with the Click-iT Plus EdU Alexa Fluor 647 Flow Cytometry Assay Kit (Invitrogen) according to manufacturer's protocol. DNA was labeled with 7-AAD (Thermo/Fisher). Data were collected using a BD LSR II Flow cytometer (BD Biosciences). Flow cytometry data were visualized with FlowJo software.

Nuclear RNA Extraction and Quality Control

NPCs were harvested at ~80% confluency with Accutase (Fisher), and nuclear fractions were prepared as described in the NE-PER Nuclear and Cytoplasmic Extraction Kit (Thermo/Fisher) manufacturer's protocol, with minor modifications. 0.5U/μl of RNase inhibitor (Ambon/Fisher) was added to the CERI reagent to prevent degradation. After separation from the cytoplasmic fraction, the nuclear pellet was washed twice with PBS (prepared in DEPC water), and resuspended in an appropriate volume of TRIzol reagent (Invitrogen). The nuclear pellet was homogenized with a Polytron PT 1200E (Kinematica). RNA was purified using the TRIzol reagent manufacturer's protocol, and quantified using the Quant-iT RNA HS Assay Kit (Invitrogen). The efficiency of separation was determined by measuring nuclear and cytoplasmic RNA fractions by qRT-PCR for the relative quantities of nuclear (*U1*) or cytoplasmic (*beta-actin*) control genes. Only nuclear RNA preparations with high *U1* expression (~8-fold nuclear increase over cytoplasm) and low *beta-actin* expression (~7-fold cytoplasmic increase over nucleus) were utilized (Figure S4). For qPCR analysis of Leptomycin B (LMB) treated NPCs, a concentration of 20nM was used for 20 hours.

qRT-PCR

RNAs, prepared as described, were reverse-transcribed to produce cDNAs using the QuantaBio qScript cDNA SuperMix (VWR) according to manufacturer's protocol, and the QuantaBio PerfeCTa SYBR® Green SuperMix (VWR) was used for quantitative real-time PCR (qRT-PCR). All reactions were run on the Applied Biosystems 7500 Fast Real-Time PCR System. The Delta-Delta-Ct method was used to compare relative transcript levels between groups. Unaffected control genes used for normalization are noted in the figure legends for each experiment.

RNA Sequencing and Analysis

RNAs were first subjected to Bioanalyzer analysis (Agilent) to assess RNA quality and concentration prior to sequencing. Libraries of nuclear fraction RNAs were prepared according to the TruSeq RNA-Seq Library protocol (Illumina). Sequencing was performed using the Illumina NextSeq500, 75SE High Output (100 million reads). Gene ontology analysis was performed using the TOPPFUN module of TOPPGENE (Chen et al., 2009). Pathway analysis was performed using Consensus PathDB (Herwig et al., 2016). The gene interaction network schematic was generated using GENEmania (Warde-Farley et al., 2010). Gene sets displayed in heatmaps were obtained from the GO term gene list as indicated within the figures. m^6A sequencing data used to generate the list of overlapping *Fmr1*/m^6A-tagged genes was reported previously (Yoon et al., 2017).

Immunoprecipitation

Cortices were harvested from *Fmr1* wild-type and KO mice and homogenized with a Kinematica Polytron PT 2500E electric homogenizer in IP buffer (20mM Tris HCl (pH8), 137mM NaCl, 1% Triton-X, 2mM EDTA) supplemented with protease inhibitor cocktail (Roche). Equal amounts of wild-type and KO lysates were used for each IP reaction, and an equal amount of wild-type lysate was used for the IgG control IP reaction. Lysates were precleared with Protein A/G PLUS Agarose beads (SCBT) for one hour at 4°C, followed by a three-hour incubation with antibody (2 μg of CRM1 or 2.75 μg of FMRP) at 4°C. Protein A/G PLUS beads were then added for an overnight 4°C incubation. Beads were washed extensively (10mM Tris (pH7.4), 1mM EDTA, 1mM EGTA, 150mM NaCl, 1% Triton-X, 0.2mM $NaVO_3$) before elution of bound IP complexes for western blot analysis. IP reactions were repeated at least three times, each time with consistent results. One representative experiment is shown. Inputs shown are 1%.

RNA Immunoprecipitation (RIP)

Starting material for each RIP reaction was ~16 million NPCs. Cells were cross-linked with ~1% EM-grade formaldehyde (Polysciences) for 15 minutes with gentle shaking. Glycine was added to a concentration of ~0.2M and shaken gently for five minutes to stop the reaction. Cells were collected, centrifuged to pellet, and resuspended in iced PBS (prepared in DEPC water). Cells were centrifuged to pellet, and washed twice more with PBS. The pellet was next resuspended in nuclear isolation buffer (0.256M sucrose, 8mM Tris HCl (pH7.5), 4mM $MgCl_2$, 1% Triton-X) and incubated on ice for twenty minutes with mixing at regular intervals. Cells were then pelleted by centrifugation, resuspended in 1 mL of RIP buffer (150mM KCl, 25mM Tris HCl (pH7.4), 5mM EDTA, 0.5mM DTT, 0.5% NP40) supplemented with protease inhibitor cocktail (Roche) and RNase inhibitors (Fisher/Ambion). Cells were sheared with twenty strokes of a glass dounce homogenizer (Wheaton), then incubated on a rotator overnight at 4°C with 4 μg of CRM1 antibody (Bethyl). Protein A Dynabeads (Invitrogen) were then added and rotated for 3 hours at 4°C. Dynabeads were pelleted using a magnetic rack and washed four times with RIP buffer, then once with PBS. Beads were resuspended in 200nM RIP buffer containing 40U/ml RNase inhibitor and 20 μg of Proteinase K (VWR), and incubated at 42°C for one hour followed by one hour at 65°C. TRIzol was then added to the beads and RNA was purified as described.

Electrophoretic Mobility Shift Assay (EMSA)

Full-length FMRP isoform 1 protein, tagged with six histidine on the amino-terminus, was purified from codon-optimized baculovirus-infected Sf9 cells by Dr. Yang Xiang at ABclonal. Biotinylated oligos were synthesized containing mouse *Dll1*mRNA sequence, 5′-GAACACCAACAAGAAGGCGGXCUUUCACGGGGXCCAUGGAGCCGA-3′ or a consensus RNA methylation sequence, 5′-CG UGGXCUGGCU-3′ (X = A or m^6A). In addition, oligos containing a mutated consensus sequence were synthesized 5′-GAUACXGA GAAG-3′. RNA probes were resuspended in DEPC-treated water and denatured by heating to 65°C for ten minutes. Recombinant FMRP protein was diluted in binding buffer (10mM HEPES, pH 8.0; 50mM KCl; 1mM EDTA; 0.05% Triton X-100; 5% glycerol; 10 μg/ml salmon sperm DNA; 1mM DTT; 40U/ml RNasin) to produce graded concentrations. One part RNA probe (20nM final concentration) was then mixed with one part protein (0nM, 125nM, 250nM, 500nM, and 1000nM final concentrations) and incubated at room temperature for thirty minutes. A rabbit anti-FMRP antibody (Cell Signaling Technology) or control rabbit IgG was added to binding reactions to induce supershift. The RNA probe-protein mixtures were run on a 4%–20% TBE gradient gel (Novex) and transferred onto a BioDYNE B nylon membrane (Fisher) using a Trans-Blot Turbo semi-dry transfer system (BioRad). The membrane was crosslinked using a UV Staratlinker 2400 (Stratagene) set to 180mg/cm^2 for 45 to 60 s. Binding was detected using the Chemiluminescent Nucleic Acid Detection Module (Fisher). Densitometry measurements of all bands were made using the measurement log feature in Adobe Photoshop to calculate the dissociation constant (K_d). Results are averaged from three independent experiments.

Bio-Layer Interferometry Analysis

Bio-layer interferometry analysis of FMRP binding to the short m^6A-modified and non-modified RNA oligos was assessed using the BLItz system (Forte Bio). Purified His-tagged FMRP (isoform 1) was loaded onto penta-His biosensors. Binding to m^6A-modified and non-modified RNA probes was recorded at the following RNA concentrations: 5000nM, 2500nM, 500nM, 150nM, and 0nM. Reagents were prepared in binding buffer containing 100mM KCl, 20mM HEPES, 1mM EDTA, 0.05% Triton-X, 5% glycerol, and 1mM DTT. Each reaction was performed using 30 s for all baselines, 120 s for loading, 120 s for association, and 120 s for dissociation. K_D was analyzed using MATLAB's nonlinear curve-fit function as described above, and reported data represent three replicates.

Western Blot

Nuclear and cytoplasmic fractions were prepared for western blot analysis according to the NE-PER Nuclear and Cytoplasmic Extraction Kit (Thermo/Fisher) protocol and supplemented with protease inhibitor cocktail (Roche). Samples were run on SDS-PAGE, followed by transfer onto PVDF membranes. Membranes were blocked for one hour at room temperature in 5% nonfat milk, incubated with primary antibodies overnight at 4°C, and incubated with secondary antibodies for one hour at room temperature. Primary antibodies were diluted in 0.01% TBS-Tween containing 5% BSA as follows: Rabbit anti-FMRP (Cell Signaling Technology, 1:1000), Rabbit anti-PTCH1 (Proteintech, 1:1000), Rat anti-DLL1 (Millipore-Sigma, 1:500), rabbit anti-CRM1 (Bethyl Labs, 1:2500), mouse anti-Fascin (Santa Cruz Biotechnology, 1:1000), mouse anti-Lamin A/C (Cell Signaling Technology, 1:500), mouse anti-beta-actin (Sigma, 1:2000), and mouse anti-beta tubulin (Fisher, 1:2000). For western blot analysis of Leptomycin B (LMB)-treated NPCs, a concentration of 40nM LMB was used for 20 hours.

Nucleofection of NPCs

*Fmr1*KO NPCs were cultured as described. Dr. Stephanie Ceman kindly provided *pEGFP-Flag-mFmr1 WT* and *pEGFP-Flag-mFmr1 ΔNES* plasmids (Kim et al., 2009). Nucleofection was performed using the Amaxa P3 Primary Cell 4D-Nucelofector X kit (Lonza) according to manufacturer's protocol. Per reaction, about six million cells and 5 μg of plasmid DNA were used. The program "DS113" was utilized for all reactions. Following nucleofection, NPCs were cultured for 24 hours prior to harvesting nuclear and cytoplasmic fractions as described. All samples used for analysis showed comparable nuclear and cytoplasmic separation based on qRT-PCR analysis, and comparable nucleofection efficiency based on GFP fluorescence.

QUANTIFICATION AND STATISTICAL ANALYSIS

Statistical analysis was performed using Prism7 software (Graphpad). Non-linear curve fitting, used to determine the dissociation constant in Figure 3B, was performed using MATLAB (MathWorks). Specific details regarding the statistical test used, number of samples (n), and number of experimental replicates are in the figure legends. All graphs present mean + SEM. For all experiments, an alpha of 0.05 was used and significance level is indicated as follows: ns $p > 0.05$, * $p \leq 0.05$, ** $p \leq 0.01$, *** $p \leq 0.001$, **** $p \leq 0.0001$. The distributions of all datasets were analyzed prior to analysis to confirm the applicability of the statistical approach (i.e., verify Normal distribution of data subjected to t test).

DATA AND CODE AVAILABILITY

Sequencing data have been deposited to the Gene Expression Database (GEO) at NCBI. Accession: GSE121809

Cell Reports, Volume *28*

Supplemental Information

FMRP Modulates Neural Differentiation through m^{6}A-Dependent mRNA Nuclear Export

Brittany M. Edens, Caroline Vissers, Jing Su, Saravanan Arumugam, Zhaofa Xu, Han Shi, Nimrod Miller, Francisca Rojas Ringeling, Guo-li Ming, Chuan He, Hongjun Song, and Yongchao C. Ma

Figure S1

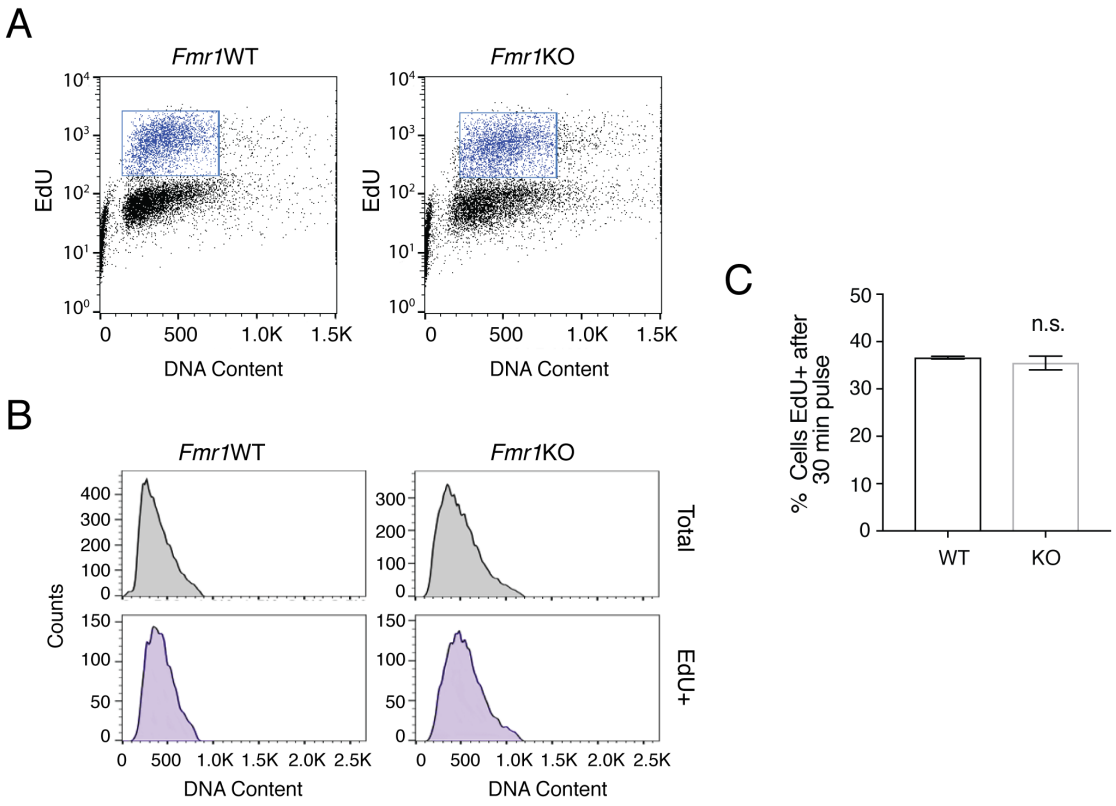

Figure S1: EdU incorporation does not differ between WT and *Fmr1*KO NPCs, Related to Figure 1.
A. FACS analysis of EdU uptake in WT and *Fmr1*KO NPCs. Cells labeled during a 30 minute EdU pulse are shown in blue.
B. Histograms comparing WT and *Fmr1*KO NPCs. The number and distribution of NPCs following a 30 minute EdU pulse is similar between WT and *Fmr1*KO.
C. There is no significant difference in the number of EdU+ cells following a thirty-minute pulse between WT and *Fmr1*KO NPCs (p=0.4623; n=6WT, 6KO).

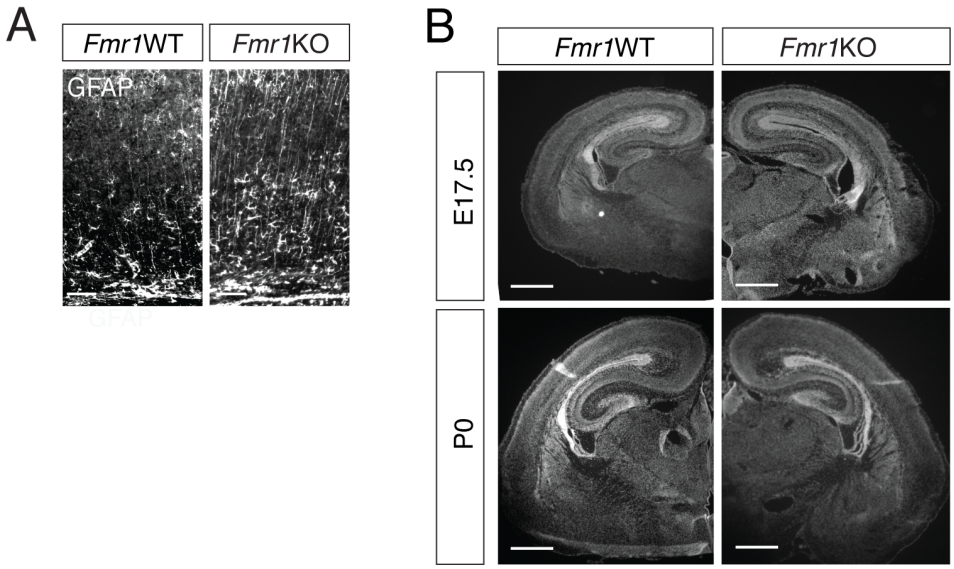

Figure S2: Radial glial fibers persist into postnatal stages in *Fmr1*KO mice, Related to Figure 2.
A. Immunostaining of GFAP in WT and *Fmr1*KO cortex at P7. Scale bar = 50μm.
B. DAPI staining of E17.5 (top) and P0 (bottom) *Fmr1*WT and *Fmr1*KO mouse cortex. Scale bar = 200μm.

Figure S3

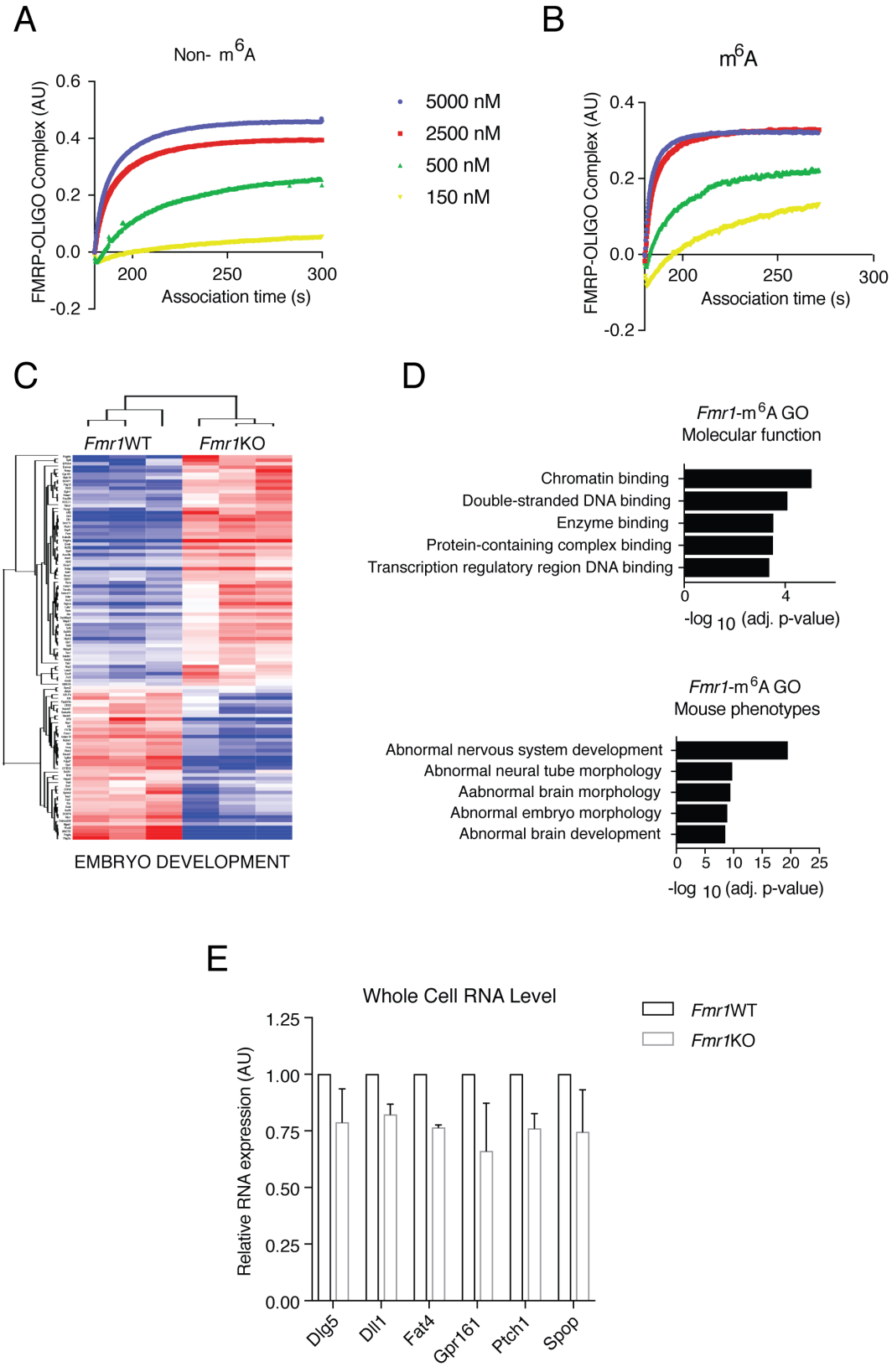
A
Non- m6A
FMRP-OLIGO Complex (AU)
0.6
0.4
0.2
0.0
-0.2
200
250
300
Association time (s)
5000 nM
2500 nM
500 nM
150 nM
B
m6A
FMRP-OLIGO Complex (AU)
0.4
0.2
0.0
-0.2
200
250
300
Association time (s)
C
Fmr1WT
Fmr1KO
EMBRYO DEVELOPMENT
D
Fmr1-m6A GO
Molecular function
Chromatin binding
Double-stranded DNA binding
Enzyme binding
Protein-containing complex binding
Transcription regulatory region DNA binding
0
4
-log 10 (adj. p-value)
Fmr1-m6A GO
Mouse phenotypes
Abnormal nervous system development
Abnormal neural tube morphology
Aabnormal brain morphology
Abnormal embryo morphology
Abnormal brain development
0 5 10 15 20 25
-log 10 (adj. p-value)
E
Whole Cell RNA Level
Fmr1WT
Fmr1KO
Relative RNA expression (AU)
1.25
1.00
0.75
0.50
0.25
0.00
Dlg5
Dll1
Fat4
Gpr161
Ptch1
Spop

Figure S3: Binding and gene expression analysis, Related to Figure 3.
A. and **B.** Bio-layer interferometry kinetic association analysis of FMRP binding to methylated (A) or non-methylated (B) RNA. Results are averaged from three independent experiments.
C. Heat map comparing WT and *Fmr1*KO nuclear expression of genes related to embryo development.
D. Gene ontology analysis of transcripts that are both m^6A-modified and differentially expressed in *Fmr1*KO nucleus. Molecular function (top) and mouse phenotypes (bottom) are shown.
E. RT-qPCR analysis of m^6A-tagged FMRP target mRNAs in whole cell WT and *Fmr1*KO RNAs (n=3WT, 3KO).

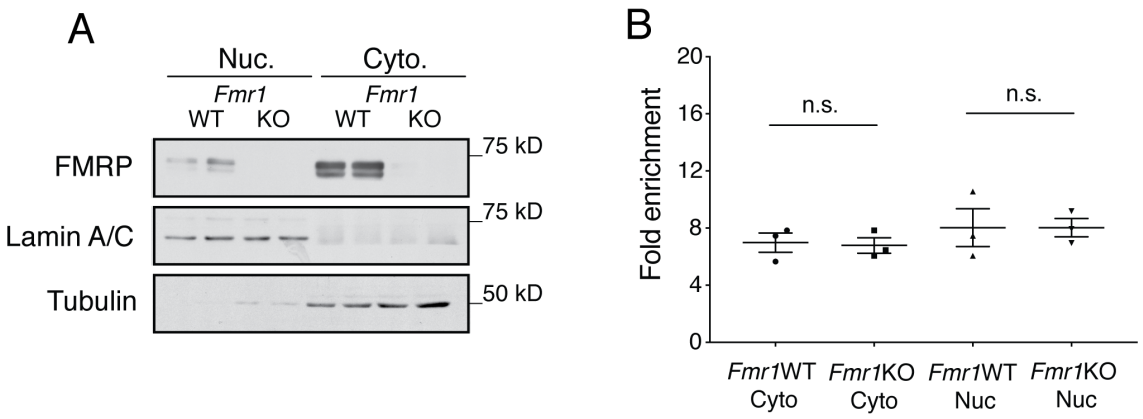

Figure S4: Nuclear fractions are efficiently separated from the cytoplasm in *Fmr1* samples, Related to Figures 3 and 4.

A. Representative Western blot demonstrating nuclear and cytoplasmic fraction separation. Lamin A/C and Tubulin serve as positive controls for nuclear and cytoplasmic fractions, respectively.

B. Comparison of nuclear (*U1*) and cytoplasmic (*beta-actin*) marker enrichment detected by RT-qPCR between fractions from WT and *Fmr1*KO NPCs prepared for RNA sequencing. Only nuclear RNA preparations with high *U1* expression (~8-fold nuclear increase over cytoplasm) and low *beta-actin* expression (~7-fold cytoplasmic increase over nucleus) were used for analysis. There are no statistical differences between different preparations of nuclear ($p=0.9974$; n=3WT, 3KO) or cytoplasmic samples ($p=0.8263$; n=3WT, 3KO).

Table S1, Primer Information, related to STAR Methods

Primer sequences for RT-qPCR analysis of Hedgehog- and Notch-related RNAs.

GENE		PRIMER SEQUENCE
Dll1	Forward	CAGGACCTTCTTTCGCGTATG
	Reverse	AAGGGGAATCGGATGGGGTT
Ptch1	Forward	AAAGAACTGCGGCAAGTTTTTG
	Reverse	CTTCTCCTATCTTCTGACGGGT
Dlg5	Forward	AAAGTGGACTGTACCTCTCTTCG
	Reverse	GTGCCGGTTCTTTTCTGTGAT
Gpr161	Forward	CTCACGCTTGGGGTCATTG
	Reverse	GAGCCAGATGTAGACGAGAGC
Spop	Forward	CCACCTCCGGCAGAAATGTC
	Reverse	CCTCCCGGCAAAAACTAAAGT
Fat4	Forward	CAGTGGTGATCCAGGTACGG
	Reverse	TCATGCGCTGTCACGGAAATA
Snora3	Forward	TCCGAGGCTAGAGTCACG
	Reverse	ATATGTCACTAACCTGGTGACTG
U1	Forward	GATACCATGATCACGAAGGTGGTT
	Reverse	CACAAATTATGCAGTCGAGTTTCC
Actb (beta-actin)	Forward	GCGAGCACAGCTTCTTTGC
	Reverse	TCGTCATCCATGGCGAACT